THE JOURNAL OF PHYSICAL CHEMISTRY C

Article

pubs.acs.org/JPCC

Chemical State, Distribution, and Role of Ti- and Nb-Based Additives on the $Ca(BH_4)_2$ System

Christian Bonatto Minella,[†,◇] Eva Pellicer,[‡] Emma Rossinyol,[§] Fahim Karimi,[†] Claudio Pistidda,[†] Sebastiano Garroni,[‡,□] Chiara Milanese,[∥] Pau Nolis,[⊥] Maria Dolors Baró,[‡] Oliver Gutfleisch,[#,○] Klaus P. Pranzas,[†] Andreas Schreyer,[†] Thomas Klassen,[†] Rüdiger Bormann,[†] and Martin Dornheim*[,†]

[†]Helmholtz-Zentrum Geesthacht, Zentrum für Material- und Küstenforschung GmbH, Institute of Materials Research, Materials Technology, Max Planck Str. 1, D-21502 Geesthacht, Germany

[‡]Universitat Autònoma de Barcelona, Departament de Física, E-08193 Bellaterra, Spain

[§]Universitat Autònoma de Barcelona, Facultat de Ciències, Servei de Microscòpia, E-08193 Bellaterra, Spain

[∥]Università degli Studi di Pavia, CSGI−Dipartimento di Chimica, Sezione di Chimica Fisica, Viale Taramelli 16, 27100 Pavia, Italy

[⊥]Universitat Autònoma de Barcelona, Servei de Ressonància Magnètica Nuclear (SeRMN), E-08193 Bellaterra, Spain

[#]IFW Dresden, Institute for Metallic Materials, Helmholtzstrasse 20, D-01069 Dresden, Germany

[○]Technische Universität Darmstadt, Materials Science, Petersenstrasse 23, 64287 Darmstadt, Germany

Supporting Information

ABSTRACT: Light metal tetrahydroborates are regarded as promising materials for solid state hydrogen storage. Due to both a high gravimetric hydrogen capacity of 11.5 wt % and an ideal dehydrogenation enthalpy of 32 kJ mol^{-1} H_2, $Ca(BH_4)_2$ is considered to be one of the most interesting compounds in this class of materials. In this work, a comprehensive investigation of the effect of different selected additives (TiF_4, NbF_5, Ti-isopropoxide, and CaF_2) on the reversible hydrogenation reaction of calcium borohydride is presented combining different investigation techniques. The chemical state of the Nb- and Ti-based additives is studied by X-ray absorption spectroscopy (e.g., XANES). Transmission electron microscopy (TEM) coupled with selected area electron diffraction (SAED) and energy-dispersive X-ray spectroscopy (EDX) was used to show the local structure, size, and distribution of the additive/catalyst. $^{11}B\{^1H\}$ solid state magic angle spinning-nuclear magnetic resonance (MAS NMR) was carried out to detect possible amorphous phases. The formation of TiB_2 and NbB_2 nanoparticles was observed after milling or upon sorption reactions of the Nb- and Ti-based $Ca(BH_4)_2$ doped systems. The formation of transition-metal boride nanoparticles is proposed to support the heterogeneous nucleation of CaB_6. The {111}CaB_6/{1011}NbB_2, {111}CaB_6/{1010}NbB_2, as well as {111}CaB_6/{1011}TiB_2 plane pairs have the potential to be the matching planes because the *d*-value mismatch is well below the *d*-critical mismatch value (6%). Transition-metal boride nanoparticles act as heterogeneous nucleation sites for CaB_6, refine the microstructure thus improving the sorption kinetics, and, as a consequence, lead to the reversible formation of $Ca(BH_4)_2$.

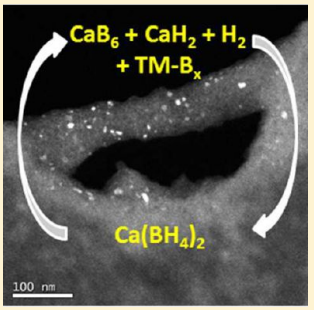

INTRODUCTION

Hydrogen is considered a promising future energy carrier due to its high abundance and its weight. In addition, its chemical energy per mass is the highest among all the chemical fuels. Solid state hydrogen storage is advantageous concerning safety and suitability compared to the liquid and compressed gas technology.[1] Alkaline and alkaline earth metal tetrahydroborates offer high gravimetric and volumetric hydrogen densities which could satisfy the requirements set by the DoE (U.S. Department of Energy).[2] Among light metal tetrahydroborates, $Ca(BH_4)_2$ is regarded as a potential candidate for solid state hydrogen storage due to its high gravimetric (11.5 wt %) and volumetric (~130 kg m^{-3}) hydrogen content.[3] In addition, the dehydrogenation enthalpy was calculated to be 32 kJ mol^{-1} H_2,[4,5] provided that CaH_2 and CaB_6 are the decomposition products, which is within the optimal range for mobile applications.[4,5] As a consequence, a decomposition temperature lower than 100 °C at 1 bar H_2 pressure is estimated. However, several decomposition paths for pure $Ca(BH_4)_2$ are reported in the literature

$$Ca(BH_4)_2 \leftrightarrow 2/3CaH_2 + 1/3CaB_6 + 10/3H_2 \quad (1)$$

$$Ca(BH_4)_2 \leftrightarrow CaH_2 + 2B + 3H_2 \quad (2)$$

$$Ca(BH_4)_2 \leftrightarrow CaB_2H_2 + 3H_2 \quad (3)$$

$$Ca(BH_4)_2 \leftrightarrow CaB_2H_6 + H_2 \quad (4)$$

Received: November 26, 2012
Revised: February 11, 2013
Published: February 12, 2013

$$Ca(BH_4)_2 \leftrightarrow 1/6CaB_{12}H_{12} + 5/6CaH_2 + 13/6H_2 \quad (5)$$

Besides CaH_2 and H_2, the decomposition of calcium borohydride could lead to the formation of boron or several boron-based compounds such as CaB_6, CaB_2H_2, CaB_2H_6, and $CaB_{12}H_{12}$.[6−9] The calculated enthalpies of reaction are 37.04,[9] 57.3,[10] 31.09,[9] and 39.2[6] or 31.34[9] kJ mol^{-1} H_2 for reactions 1, 2, 4, and 5, respectively. These values are calculated at 300 K and 1 bar H_2 pressure. For reaction 3, a reaction enthalpy value of 68.51 kJ mol^{-1} H_2 was calculated at 0 K ignoring the zero-point energy.[9]

Upon decomposition of tetrahydroborates, formation of $[B_{12}H_{12}]^{2-}$ containing species were predicted to be plausible in particular due to their high chemical stability.[6,11] However, their detection is complicated. The existence of several amorphous polymorphs of $CaB_{12}H_{12}$ was predicted upon desorption of $Ca(BH_4)_2$ (reaction 5).[8] The enthalpies of reaction of such phases are almost degenerate (ΔH^{0K} = 35.8−37.9 kJ mol^{-1} H_2).[8] Formations of CaB_2H_x (x = 2) (reaction 3) and of the CaB_mH_n phase were recently observed.[12,13] By calculations, Zhang et al.[9] found that the CaB_2H_x (x = 2) phase is too unstable to be a decomposition product of calcium borohydride (decomposition enthalpy ca. 50 kJ mol^{-1} H_2 > CaB_2H_6 and $CaB_{12}H_{12}$). They showed, by density functional theory (DFT) and prototype electrostatic ground state (PEGS) calculations, the CaB_2H_6 phase to be more probable (reaction 4).[9] They also demonstrated that when vibrational entropy and free energy (including ZPE, zero-point energy) are taken into account the reaction enthalpy value of CaB_2H_6 (reaction 4) competes in energy with that of $CaB_{12}H_{12}$ (reaction 5) within 1 kJ mol^{-1} H_2.[9]

Rehydrogenation attempts on the decomposition products of undoped $Ca(BH_4)_2$ did not lead to its reversible formation.[14,15] Unsuccessful reversibility in the pure $Ca(BH_4)_2$ system is likely related to formation of both boron (reluctant to react even in harsh conditions) and $[B_{12}H_{12}]^{2-}$ phases upon desorption and slow mass transport of boron-containing phases upon rehydrogenation although a high hydrogen pressure was applied.[14−16]

Transition- and light-metal based additives have shown to be beneficial on the sorption reaction kinetics of complex hydrides.[17,18] Transition-metal chlorides and fluorides, in particular, are highly reactive. They likely evolve to more stable compounds when combined with a hydride phase during mechanical treatment or during sorption reactions.[19] For instance, $Ca(BH_4)_2$ was synthesized with a yield of 60% from a mixture of CaH_2 and CaB_6 with Pd and $TiCl_3$ by applying 700 bar H_2 and temperatures of 400−440 °C.[20] $Ca(BH_4)_2$ was also obtained (yield of 19%)[21] by high-pressure reactive ball milling of CaH_2 and CaB_6 after 24 h at 140 bar H_2 employing TiF_3 or $TiCl_3$ as additives. Lately, some transition-metal fluorides and chlorides ($TiCl_3$, NbF_5, and TiF_4) have demonstrated to positively affect its partial reversible formation in milder experimental conditions.[14,22,23]

The reasons for the beneficial effect provided by transition-metal fluoride additives on the reversible formation of $Ca(BH_4)_2$ are not yet entirely explained. In general, the multivalency of transition metals could favor electronic exchange reactions with hydrogen molecules, accelerating the gas−solid reaction. In addition, due to their high reactivity, transition-metal fluorides react during milling or desorption leading to the formation of transition-metal-based nanoparticles. The nanoparticles, when homogeneously distributed in the matrix, could favor mass transport and retention of the crystallite size within the nanometer scale and might act as heterogeneous nucleation agents of compounds like CaB_6 (suppressing boron formation). In addition, the presence of fluorine phases on the surface of the tetrahydroborate could accelerate the reaction with hydrogen as already reported for other systems.[24−26]

To monitor the evolution of the transition-metal fluoride additives upon cycling, X-ray-based techniques emerged as powerful tools. Friedrichs et al.,[27−29] Deprez et al.,[30,31] and Bösenberg et al.[32,33] applied them to understand the role of additives in both MgH_2 and the $LiBH_4$ + MgH_2 reactive hydride composite system.

In this study, the chemical state of the Nb- and Ti-based additives was investigated by X-ray absorption near edge structure (e.g., XANES). Transmission electron microscopy (TEM) coupled with selected area electron diffraction (SAED) or energy-dispersive X-ray spectroscopy (EDX) was used to reveal the local structure, size, and distribution of the additive/catalyst. $^{11}B\{^1H\}$ solid state magic angle spinning-nuclear magnetic resonance (MAS NMR) was carried out to detect possible amorphous phases. Since the addition of NbF_5 and TiF_4 additives to $Ca(BH_4)_2$ promoted a side reaction to form CaF_2 upon milling, a set of experiments adding solely CaF_2 to $Ca(BH_4)_2$ were conducted. In this way, any effect provided by CaF_2 on the reversible formation of $Ca(BH_4)_2$ should be clarified. Finally, we discuss the ability of transition-metal boride nanoparticles to support the heterogeneous nucleation of CaB_6, considered to play a key role for the reversible formation of $Ca(BH_4)_2$ and their function as a grain refiner during sorption reactions.

EXPERIMENTAL METHODS

$Ca(BH_4)_2$ powder was obtained by drying the commercially available $Ca(BH_4)_2$·2THF adduct (purchased from Sigma-Aldrich) for 1 h and 30 min at 200 °C in a vacuum and subsequent cooling to room temperature. Four different samples were prepared adding 5 mol % of TiF_4 (purity 98%), NbF_5 (purity 99%), titanium isopropoxide (99.995% purity), and 5 wt % of CaF_2 (99.99% purity), purchased from Sigma-Aldrich, to $Ca(BH_4)_2$. The samples were milled in a stainless steel vial in argon atmosphere for 1 h and 40 min using a Spex Mixer Mill (model 8000) and 14:1 as ball to powder ratio (four spheres of 3.5 g of each one and 1 g of powder). All powder handling and milling was performed in an MBraun argon box with H_2O and O_2 levels below 10 ppm to prevent contamination.

Sorption properties and kinetics were evaluated by thermovolumetric measurements using a Sievert-type apparatus designed by a Hydro Quebec/HERA Hydrogen Storage System. The milled powders (70−90 mg) were desorbed by heating from room temperature (25 °C) up to 450 °C in a static vacuum (0.02 bar starting pressure) and subsequently reabsorbed at 350 °C and 145 bar H_2 for 20−24 h.

X-ray absorption near edge structure (XANES) measurements of the $Ca(BH_4)_2$ samples with 5 mol % of TiF_4 and NbF_5 were performed in transmission mode at the synchrotron Hasylab, DESY (Hamburg), at the beamline A1 and C, respectively. Spectra were collected at the Ti and Nb K-edge (4966 and 18986 eV, respectively) under vacuum at ambient temperature. The beamlines are equipped with a Si(111) channel cut double crystal monochromator. In addition, beamline A1 has a two-mirror system (the first mirror is

dx.doi.org/10.1021/jp3116275 | J. Phys. Chem. C 2013, 117, 4394−4403

coated with Ni, and the second mirror has two stripes, one coated with Ni and the other one uncoated SiO_2) to suppress higher harmonic rejection. The as-milled and dehydrogenated/rehydrogenated samples were mixed with cellulose powder for dilution before experiments. The mixed powders were pressed to pellet shape and placed between two Kapton foils on aluminum sample holders. This procedure was performed in an argon-filled glovebox. Ti foil, TiB_2, Ti_2O_3, TiO_2 (anatase), TiO, TiF_3, and TiF_4 samples were used as a reference for the measurements at the Ti K-edge. Nb-foil, NbO, NbF_5, NbB_2, and Nb_2O_5 samples were used as a reference for the measurements at the Nb K-edge. EXAFS data processing was carried out by the software ATHENA and ARTHEMIS[34] two interactive graphical utility based on the IFFEFIT[35] library of numerical and X-ray absorption spectroscopy algorithms. XANES data analyses were performed subtracting the pre-edge background and normalizing the edge.

TEM characterization, including bright and dark field imaging and selected area electron diffraction (SAED), was conducted on a Jeol-JEM 2011 microscope operating at 200 kV. The powders were dispersed in THF under Ar atmosphere in a glovebox, and then a couple of drops were placed dropwise onto a holey carbon supported grid. To prevent oxidation, the sample holder was immediately inserted into the microscope (i.e., before the solvent was completely evaporated). Elemental chemical analyses were performed with an energy dispersive X-ray spectroscopy (EDX) system coupled to the TEM microscope.

X-ray diffraction patterns were collected at the synchrotron MAX-lab, Lund (Sweden), at the beamline I711.[36] The beamline is equipped with a MAR165 CCD detector. Quartz capillaries with 1.0 or 0.7 mm outside diameter were filled with powder, closed with candle wax to avoid contamination by oxygen or water, and then exposed to the beam for 15 or 30 s. Longer exposures (240−360 s) were performed on some selected samples to improve the resolution. The relative phase abundances are calculated using the Rietveld method (by MAUD software).[37] For comparison purposes, all X-ray diffraction data are referred to the scattering vector $4\pi \sin\theta\lambda^{-1}$ ($Å^{-1}$).

The one-dimensional ^{11}B magic angle spinning-nuclear magnetic resonance ((1D) $^{11}B\{^1H\}$ MAS NMR) measurements were obtained using a Bruker Avance 400 MHz spectrometer with a wide bore 9.4 T magnet and employing a boron-free Bruker 4 mm CPMAS probe. The spectral frequency was 128.33 MHz for the ^{11}B nucleus, and the NMR shifts are reported in parts per million (ppm) externally referenced to BF_3Et_2O. The powder materials were packed into 4 mm ZrO_2 rotors in an argon-filled glovebox and were sealed with tight fitting Kel-F caps. The one-dimensional (1D) $^{11}B\{^1H\}$ MAS NMR spectra were acquired after a 2.7 μs single $\pi/2$ pulse (corresponding to a radio field strength of 92.6 kHz) and with application of a strong ^1H signal decoupling by using the two-pulse phase modulation (TPPM) scheme. The spectra were recorded at a MAS spinning rate of 12 kHz. Sample spinning was performed using dry nitrogen gas. The recovery delay was set to 10 s. Spectra were acquired at 20 °C (controlled by a BRUKER BCU unit). For comparison purposes, the $^{11}B\{^1H\}$ MAS NMR spectrum of the $CaB_{12}H_{12}$ is reported as well. It was synthesized following the procedure reported by Bonatto Minella et al. in reference 16.

RESULTS AND DISCUSSION

The nature of the Nb phase as well as its oxidation state during sorption reactions was determined by XANES. XANES data measured at the Nb K-edge (18986 eV) are shown in Figure 1.

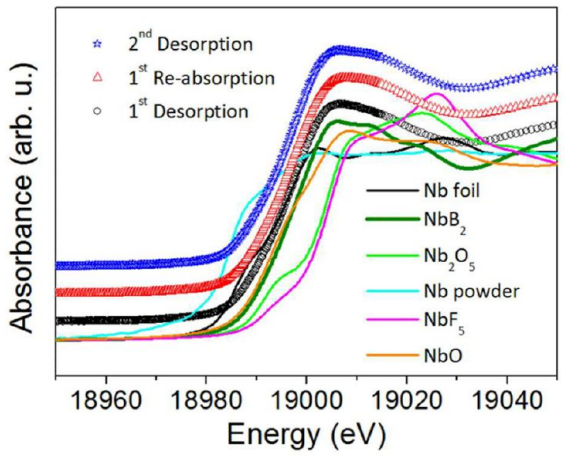

Figure 1. XANES data at the Nb K-edge for $Ca(BH_4)_2 + NbF_5$ (with 5 mol % NbF_5) material after first desorption (black ○), after subsequent reabsorption (red △), and after second desorption (blue ☆).

The figure includes the spectrum of the material after first desorption, after subsequent reabsorption, and after second desorption reaction. A direct comparison between the curve of the desorbed material and that of the pure NbF_5 additive indicates that a reaction, involving the additive itself and $Ca(BH_4)_2$ has occurred. The XRD in Figure 1A (Supporting Information) evidences formation of CaF_2 after milling which indicates that a reaction between NbF_5 and $Ca(BH_4)_2$ has taken place already during the mechanochemical process. In fact, NbF_5 is characterized by a low melting temperature (mp 79 °C), and values of ca. 100 °C can be reached inside the vial during milling.[38] This would increase the reactivity of NbF_5 as demonstrated by studies on the composition of its vapor pressure at these temperatures.[39] Moreover, a reaction between transition-metal fluorides and $Ca(BH_4)_2$, occurring in the 125−225 °C temperature range, has already been reported in the literature.[14] Furthermore, the curves of the material after reabsorption and after second hydrogen desorption show no further change in the oxidation state of Nb over cycling. The shift toward lower energy of the Nb K-edge in the desorbed sample, compared to the NbF_5 additive, indicates that the oxidation state of the Nb species reduces irreversibly. The irreversible reduction is confirmed observing the curves after reabsorption and second desorption which are comparable to that after first dehydrogenation. Figure 1 shows that the curves belonging to the desorbed/reabsorbed materials fairly match that of the pure NbB_2, measured as a reference compound. This would indicate a reduction of the oxidation state for the Nb species from (V) to (II). In addition, a similar profile for the curves belonging to the desorbed/reabsorbed materials and for the NbB_2 along the EXAFS (extended X-ray absorption fine structure) region (at higher energies with respect to the Nb absorption K-edge) would suggest a Nb−B bond in the first coordination shell. However, this assumption needs to be confirmed by Fourier transform analysis of the EXAFS data. No trace of the NbB_2 phase can be observed in the X-ray diffraction

dx.doi.org/10.1021/jp3116275 | J. Phys. Chem. C 2013, 117, 4394−4403

patterns of the NbF_5 doped $Ca(BH_4)_2$ material after milling, desorption, or reabsorption (Supporting Information, Figures 1 and 2).[14] The dimension of such boride particles can be in the range of a few nanometers and hence below the detection range of X-ray diffraction techniques.[32] Nevertheless, as described above, the formation of NbB_2 nanoparticles, in the case of the NbF_5 additive, is believed to occur already during the milling process.

XANES analysis at the Ti K-edge (4966 eV), including the curve for the ball-milled and desorbed material, is reported in Figure 2.

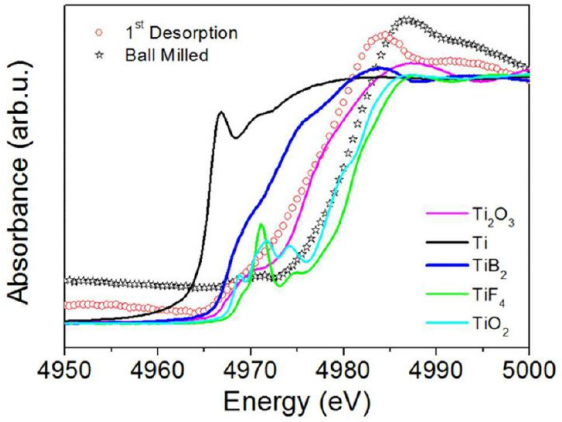

Figure 2. XANES data at the Ti K-edge for the milled $Ca(BH_4)_2$ + TiF_4 (with 5 mol % TiF_4) material after ball milling (black ☆) and first desorption (red ○).

A comparison, in the pre-edge region of the spectra, among the curve of the ball-milled material and those of TiF_4, TiO_2, and Ti_2O_3, suggests that a reaction, involving TiF_4 and $Ca(BH_4)_2$, has taken place inside the vial already during the milling process. In fact, the pre-edge at 4971 eV for the TiF_4 curve has disappeared in the case of the milled sample. The reaction between TiF_4 (as well as in the case of NbF_5) and $Ca(BH_4)_2$ was already observed upon desorption.[14] The Ti absorption K-edge, in the case of the milled sample, matches the value observed for TiO_2, Ti_2O_3, and TiF_4. The presence of TiF_4 after milling is unlikely since XRDs (Supporting Information, Figure 2A), beside γ-$Ca(BH_4)_2$ and β-$Ca(BH_4)_2$, show the presence of CaF_2 which should be caused by a reaction between $Ca(BH_4)_2$ and TiF_4. However, a fraction of TiF_4 which might still be present due to the milling in nanometer size, would be hard to detect using X-rays. In addition, within the rising edge region of Figure 2 (at higher energies compared to the pre-edge region) the curve of the milled sample overlaps that of pure TiF_4. Given the formation enthalpy data and considering the high sensitivity of alkali tetrahydroborates to moisture,[40] formation of Ti_2O_3 seems to be likely. In addition, Riktor et al.[41] reported the starting $Ca(BH_4)_2$ material containing already solvent traces or oxygen-containing impurities. Nevertheless, within the rising edge region, the curve of the milled sample is closer to that of pure TiO_2 than that of Ti_2O_3. Experiments performed by Buslaev et al.[42] would exclude TiO_2 as a product of the hydrolysis reaction of TiF_4. The combination of the observations reported for the milled sample, at the pre-edge region, at the rising edge region, and at the absorption edge allows concluding that Ti has an oxidation state of IV (TiO_2 or TiF_4).

The desorbed sample shows a reduction in the oxidation state of Ti. The Ti absorption K-edge, in the case of the desorbed sample, matches the value observed for TiB_2. Within the rising edge region, the curve of the desorbed sample fits that of pure Ti_2O_3. The combination of these observations allows concluding that either Ti has an oxidation state between III (Ti_2O_3) and II (TiB_2) or a mixture of both different chemical states. The same behavior was already reported by Deprez et al.[30] in the case of the Ti-isopropoxide doped $LiBH_4$–MgH_2 reactive hydride composite system.

TEM microscopy of the desorbed $Ca(BH_4)_2$ samples doped with NbF_5 and TiF_4 was carried out to confirm the presence of the transition-metal boride nanoparticles and their size in the desorbed/reabsorbed materials. Actually, the formation of transition-metal boride nanoparticles upon the hydrogen desorption reaction, in the case of doped systems, is more than a certainty, and it would be consistent with several works recently reported in the literature.[30,32,33,43] The TEM pictures for the desorbed sample doped with NbF_5 are reported in Figure 3.

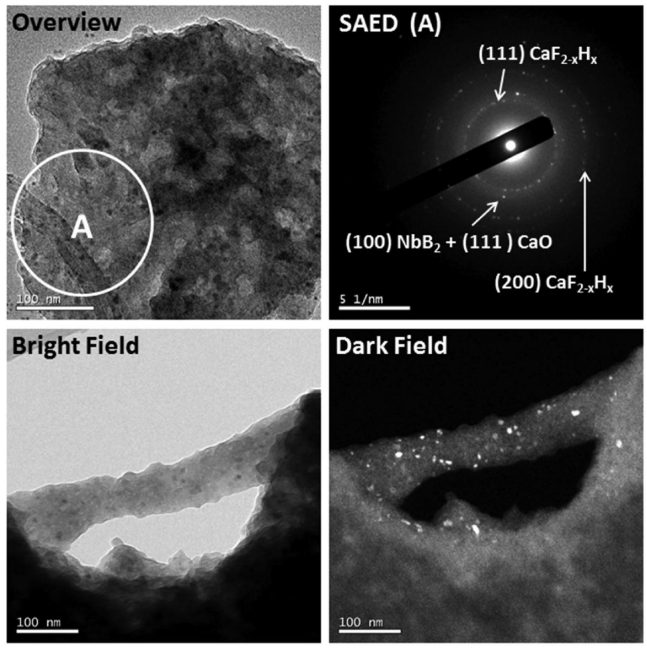

Figure 3. TEM images (bright and dark field) together with SAED analysis of the $Ca(BH_4)_2$ sample doped with NbF_5 fully desorbed at 450 °C in vacuum.

Detection of the nanoparticles was, though, complex because the powder decomposes within a few seconds due to the influence of the electron beam. Moreover, whenever the magnification was increased to obtain a better picture, the contrast decreased significantly. To bypass these issues, another approach was undertaken. Since the nanoparticles are crystalline, the investigation in dark field mode could provide pictures with a better contrast.

Figure 3 (overview) shows dark spots dispersed within the matrix of the desorbed materials, corresponding to the NbB_2 nanoparticles. This is confirmed by SAED performed in the area indicated as A in Figure 3 (overview). The SAED analysis reveals the presence of $CaF_{2-x}H_x$, CaO, and NbB_2 (Figure 3 SAED). $CaF_{2-x}H_x$ was already demonstrated to be a product of the desorption reaction between CaH_2 and CaF_2.[14] $CaB_{12}H_{12}$

dx.doi.org/10.1021/jp3116275 | J. Phys. Chem. C 2013, 117, 4394–4403

cannot be detected due to its amorphous nature. Its presence was confirmed by ^{11}B $\{^{1}H\}$ MAS NMR experiments (Supporting Information, Figure 3E).[14] Pictures in bright and dark field mode, respectively, correspond to another region of the sample. The picture collected in dark field mode, in particular, highlights the nanoparticles within the desorbed materials as bright spots. The average size of the NbB_2 nanoparticles is around 10 nm. The lighter gray zone in the dark field image that embeds the nanoparticles is representative of amorphous phases ($CaB_{12}H_{12}$). We can exclude that the bright spots correspond to the $CaF_{2-x}H_x$ or CaO phase because, as reported in the XRD pattern after decomposition (Supporting Information, Figure 1B), they exist in much bigger size. Instead, no trace of NbB_2 is visible in the same XRD pattern (Supporting Information, Figure 1B), implying that either its Bragg peaks overlap with reflections belonging to other phases or its concentration is below the detection limit of the technique itself (ca. 4 wt %).

The TEM pictures for the desorbed sample doped with TiF_4 are reported in Figure 4.

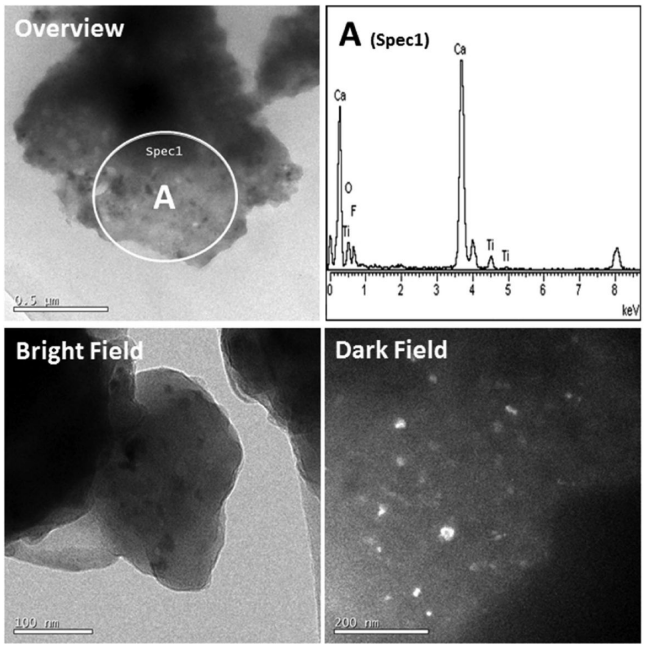

Figure 4. TEM images (bright and dark field) together with EDX analysis of the $Ca(BH_4)_2$ sample doped with TiF_4 fully desorbed at 450 °C in vacuum.

The bright field image shows dark spots dispersed within the matrix of the desorbed materials. The EDX analysis performed in the selected area (A Spec1) shows the Ca and Ti signals. The first arises from the $CaF_{2-x}H_x$, CaO (Supporting Information, Figure 2), and $CaB_{12}H_{12}$ phases (Supporting Information, Figure 3F), whereas the latter refers to either TiB_2 or Ti_2O_3 nanoparticles. Elemental boron cannot be detected by the EDX technique because it is too light. Although the detector window would be wide enough to show a boron peak, its quantification is very difficult. Fluorine and oxygen peaks are visible as well. Regrettably, SAED patterns could not be taken on the sample due to its instability under the beam. In any case, images in bright and dark field mode unambiguously reveal the presence of nanoparticles as for the NbF_5 doped sample. These nanoparticles are likely made of TiB_2 because the oxygen content is very low (i.e., it is not large enough to promote the formation of Ti_2O_3 nanoparticles). The average nanoparticle size estimated from the dark field image is approximately 20 nm.

Since the addition of TiF_4 and NbF_5 additives led to the formation of CaF_2 during milling with $Ca(BH_4)_2$ (Supporting Information, Figure 1A and 2A), two critical experiments adding either Ti-isopropoxide or CaF_2 were performed to rule out or confirm any beneficial effect provided by CaF_2 on the reversible formation of $Ca(BH_4)_2$. The first additive is a fluorine-free compound, whereas the latter does not contain any transition metal. In this way, it should be possible to shed some light on the reabsorption mechanism.

The X-ray diffraction pattern for $Ca(BH_4)_2$ milled with 5 mol % of Ti-isopropoxide is shown in Figure 5 (milled). The

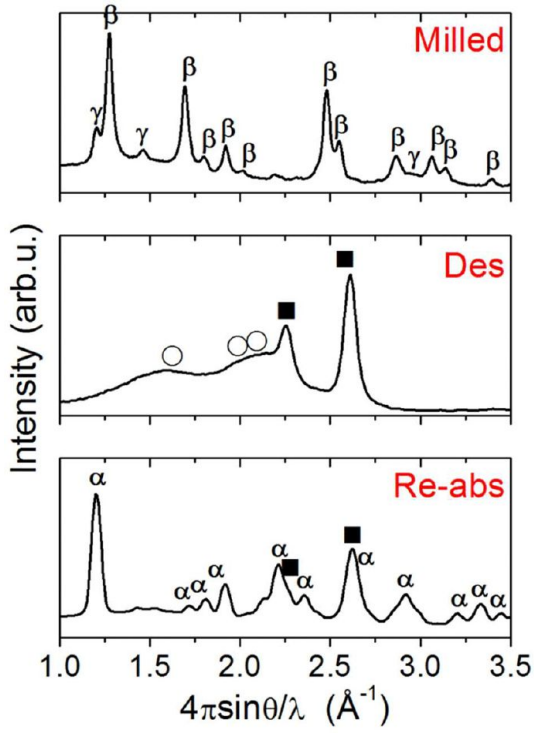

Figure 5. X-ray diffraction patterns of $Ca(BH_4)_2$ milled with 5 mol % of Ti-isopropoxide after milling (Milled), after desorption (Des), after rehydrogenation (Reabs). γ-$Ca(BH_4)_2$ (γ); β-$Ca(BH_4)_2$ (β); α-$Ca(BH_4)_2$ (α); CaH_2 (○); CaO (■).

pattern indicates simultaneous presence of γ-$Ca(BH_4)_2$ and β-$Ca(BH_4)_2$ with 7 wt % (±5 error) and 93 wt % (±5 error) abundance, respectively. The diffractogram does not show any reflection corresponding to the Ti phase or oxide that might have formed by reaction of $Ca(BH_4)_2$ with the oxygen groups of the organometallic additive. The desorption products (450 °C in vacuum) are reported in Figure 5 as well. CaH_2 and CaO are the only visible phases. The pattern does not show any trace of CaB_6. However, the intense background in the scattering value range of 1.25−2.25 (Å^{-1}) would suggest its existence among the desorption products. In fact, CaO is often present in the desorption products of $Ca(BH_4)_2$ even though the powder handling is performed in a protected atmosphere (argon). As already mentioned, Riktor et al.[41] reported that the starting $Ca(BH_4)_2$ material already contains solvent traces or oxygen-containing impurities. The desorbed materials were reabsorbed

dx.doi.org/10.1021/jp3116275 | J. Phys. Chem. C 2013, 117, 4394−4403

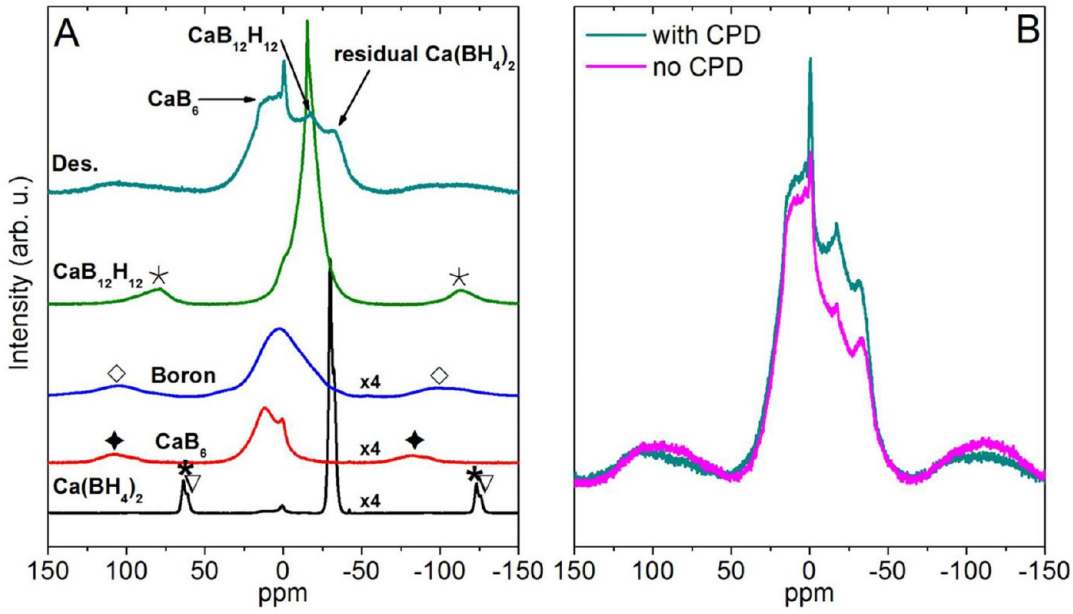

Figure 6. (A) (Des.): $^{11}B\{^1H\}$ MAS NMR spectra at room temperature of $Ca(BH_4)_2$ milled with 5 mol % of Ti-isopropoxide after first hydrogen desorption reaction (at 450 °C in vacuum). $Ca(BH_4)_2$, CaB_6 and boron, scale adjusted by 1/4. Side bands are indicated by ×, ★, ♦, ◊, ☆. (B) $^{11}B\{^1H\}$ (dark cyan) and ^{11}B (magenta) MAS NMR spectra at room temperature of $Ca(BH_4)_2$ milled with 5 mol % of Ti-isopropoxide after the first hydrogen desorption reaction (at 450 °C in vacuum) collected with and without composite-pulse decoupling (CPD).

at 350 °C and 145 bar H_2 for 24 h. The XRD pattern after reabsorption reaction is shown in Figure 5 (Reabs). The reflections of the α-$Ca(BH_4)_2$ phase are present, which proves the reversibility of the reaction. Besides, the crystallographic peaks of the CaO phase are also present. The oxygen groups contained within the Ti-isopropoxide additive probably contributed to favor the formation of CaO, although it should be taken into account that oxygen was already present in the starting $Ca(BH_4)_2$ material.[41]

$^{11}B\{^1H\}$ MAS NMR was carried out on the powder after first hydrogen desorption reaction with the aim of identifying the nature of the final B-containing compounds. The spectrum of the desorbed material is shown in Figure 6A together with those of the reference compounds.

In Figure 6A, the spectrum of desorbed $Ca(BH_4)_2$ + Ti-isopropoxide material shows a series of four signals: ∼+12 ppm, ∼−0.6 ppm, ∼−17 ppm, and ∼−32 ppm. By comparison with the spectra of the reference compounds, we can associate the peak at +12 ppm to CaB_6 and the one at −30 ppm to residual β-$Ca(BH_4)_2$. The peak at ∼−17 ppm corresponds to $CaB_{12}H_{12}$. The signals of the desorbed material are slightly shifted with respect to the values observed for the reference compounds. The values might shift as a function of the disordered nature of the phase structure.[44] The narrow signal at −0.6 ppm falls in the range of chemical shift corresponding to a BH_3-L (L = ligand) compound. The profile of the NMR spectrum in Figure 6A for the desorbed material, apart from the peak at −0.6 ppm, is very similar to those of the desorbed NbF_5 and TiF_4 doped $Ca(BH_4)_2$ materials. This signal was never observed in the case of the transition-metal fluoride doped samples. It is worth noting that the $^{11}B\{^1H\}$ MAS NMR analysis was performed on a one-year old sample, and although material storage was done in the best conditions possible, contamination by moisture cannot be completely excluded in one-year time. In addition, as aforementioned, oxygen contamination is typical in the starting $Ca(BH_4)_2$ powder.[41] In addition, it is accepted that carrier artifacts might arise in the instrument employed for this measurement, although, so far, none of them was observed. The measurement of the relaxation time T_1 and T_2 would provide more information about the chemical identity of the peak, but unfortunately it could not be carried out. Nevertheless it has to be mentioned that this particular signal only occurs in this spectrum. Usually artifacts have a different phase compared to the rest of the spectral lines. Furthermore its intensity is very noticeable compared to the spectral noise. To clarify the nature of the bond characterizing the compound giving a signal at −0.6 ppm, the NMR experiment was repeated, on the same desorbed powder, without composite-pulse decoupling (CPD).[45] The result is reported in Figure 6B. If the material contains a B−H bond a considerable decrease of the intensity of its peak should be observed. By contrast, if it does not contain the B−H bond, the intensity of the peak should decrease slightly. Figure 6B highlights how the peaks at ∼−17, at ∼−32, and at −0.6 ppm decrease their intensity by a similar proportional value, whereas the signal at ∼+12 ppm does not show the same decrement. The latter signal (+12 ppm) belongs to the CaB_6 phase, and since it does not contain B−H bonds its intensity, in both experiments, is comparable. The peaks at ∼−17 and ∼−32 ppm are known containing B−H bonds ($CaB_{12}H_{12}$ and β-$Ca(BH_4)_2$, respectively). The NMR experiment confirms that the signal at −0.6 ppm belongs to a BH_3-L (L = ligand) compound. Unfortunately, the identification of the ligand is not easy, and considering the fact that it might be due to contamination, it is not relevant.

The TEM pictures for the reabsorbed Ti-isopropoxide doped sample are reported in Figure 7 together with SAED analysis. As for the TiF_4 doped sample, detection of the nanoparticles was complex due to the instability of the material under the electron beam. The powder decomposes within a few seconds.

Figure 7 (overview) shows a general view of the sample. SAED, performed in the area indicated as A, shows the diffraction spots of the α-$Ca(BH_4)_2$, CaO, and TiB_2 phases.

dx.doi.org/10.1021/jp3116275 | J. Phys. Chem. C 2013, 117, 4394−4403

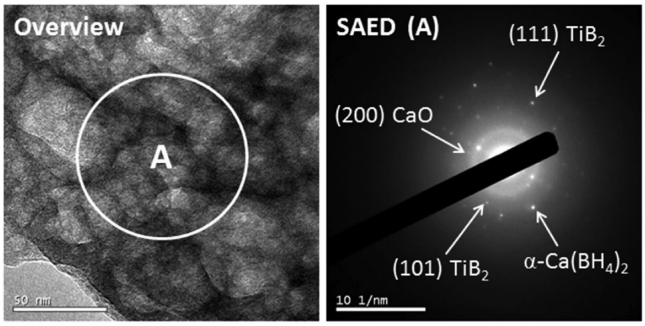

Figure 7. TEM images (bright field) together with SAED analysis of the $Ca(BH_4)_2$ sample doped with 5 mol % of Ti-isopropoxide after reabsorption.

Also in this case, the XRD (Figure 5) does not show any reflection belonging to TiB_2 likely because either its Bragg peaks overlap with reflections belonging to other phases or its concentration is below the detection limit of the technique itself (ca. 4 wt %).

The X-ray diffraction pattern for the $Ca(BH_4)_2$ milled with 5 wt % of CaF_2 is shown in Figure 8 (milled). Rietveld analysis

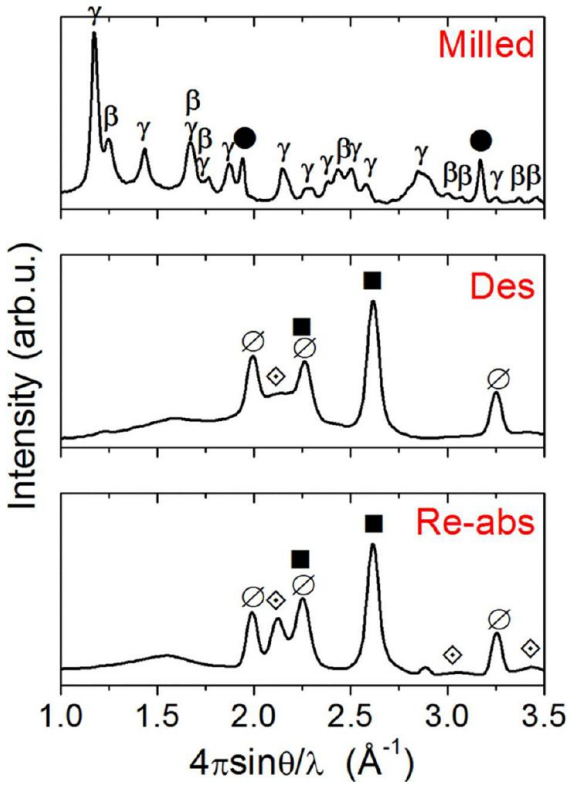

Figure 8. X-ray diffraction patterns of $Ca(BH_4)_2$ milled with 5 wt % of CaF_2 after milling (Milled), after desorption (Des), and after rehydrogenation (Reabs). γ-$Ca(BH_4)_2$ (γ); β-$Ca(BH_4)_2$ (β); α-$Ca(BH_4)_2$ (α); CaF_2 (●); $CaF_{2-x}H_x$ (⌀); CaB_6 (◊); CaO (■).

on the sample after milling indicates the presence of γ-$Ca(BH_4)_2$, β-$Ca(BH_4)_2$, and CaF_2 with 58 (±5 error), 35 (±5 error), and 7 wt % (±5 error) phase abundance, respectively.

The desorption products (450 °C in vacuum) are reported in Figure 8 (Des). The X-ray pattern evidences the peaks of the $CaF_{2-x}H_x$, CaO, and CaB_6 phase. Furthermore, Figure 8 (Des) shows a broad amorphous like peak around 1.5 Q (Å^{-1}) which suggests the presence of nanocrystalline or amorphous phases. Rietveld analysis of the pattern shown in Figure 8 (Des) was not performed. The presence of amorphous phases which cannot be detected by XRD would contribute to overestimate the values of the phase abundance. The desorbed materials were reabsorbed at 350 °C and 145 bar H_2 for 24 h. The X-ray diffraction pattern is reported in Figure 8 (Reabs). The figure still shows the crystallographic peaks of the dehydrogenated phases ($CaF_{2-x}H_x$, CaO, and CaB_6) evidencing that no reabsorption reaction has occurred. In the XRD pattern (Reabs), the peak at 2.12 Q (Å^{-1}) of the CaB_6 phase is more intense compared to the pattern (Des). The long exposure time (24 h) to both high temperature and pressure influences the peak coarsening. Furthermore, the broad peak around 1.5 Q (Å^{-1}) is still present, and it might suggest the existence of nanocrystalline or amorphous-like phases.

In the case of the $LiBH_4$−MgH_2 composite system, Bösenberg et al.[33] showed that transition-metal borides act as heterogeneous nucleation sites for the formation of MgB_2. Yet, Bösenberg et al.,[32] in the case of Zr-isopropoxide addition to the $LiBH_4$−MgH_2 composite system, report that ZrB_2 nanoparticles are located in the interfaces and grain boundaries. Transition-metal borides and MgB_2 have the same crystal structure (hexagonal), and therefore the borides provide coherent interfaces for nucleation, regardless of crystallographic planes and ledges, favoring heterogeneous nucleation of MgB_2. In our study, TEM images in dark field mode coupled with selected area electron diffraction reveal the presence of the nanoparticles and show their good distribution within the matrix. However, the pictures cannot say whether the nanoparticles lie in the grain boundaries. To provide such information, high-resolution TEM should be carried out. However, the rapid decomposition of the powder under the electron beam would not make it trivial. Nevertheless, the localization of the transition-metal boride nanoparticles in the grain boundaries might be sound since sorption reactions involve considerable mass transport which could have moved the nanoparticles to the interfaces.

The following part discusses the ability of transition-metal boride nanoparticles to support heterogeneous nucleation of CaB_6, considered to play a key role for the reversible formation of $Ca(BH_4)_2$, and their function as a grain refiner during sorption reactions. Transition-metal borides (hexagonal) and CaB_6 (cubic) have a different crystal structure. However, the borides could still provide interfaces with low interfacial energy supporting heterogeneous nucleation of CaB_6.

A fundamental requirement for heterogeneous nucleation is a low interfacial energy. Other necessary requirements for an efficient heterogeneous nucleation are a good distribution of the nucleation agents as well as a sufficient amount of it. Generally, chemical contributions are considered to play a secondary role,[46] and therefore they will be neglected in this study as was done for the doped $LiBH_4$−MgH_2 composite system.[33]

Across an interface, the maximum probability to observe atom row matching in consecutive atom rows is maximized if the planes which contain the atom rows in the two phases have very similar interplanar *d*-spacings and are arranged to meet edge-to-edge at the interface.[47,48] The planes usually considered are the close-packed or nearly close-packed. A close-packed plane corresponds, in an XRD pattern, to the plane with the highest X-ray diffraction intensity.[47,48]

dx.doi.org/10.1021/jp3116275 | J. Phys. Chem. C 2013, 117, 4394−4403

The relative difference in the *d* spacing of any two close-packed or nearly close-packed planes between two phases is called *d*-value mismatch. If the *d*-value mismatch is below a critical value (PCV), then this plane pair has potential to form orientation relationships (ORs). In our case, a *d*-critical mismatch value below or equal to 6% is considered reasonable.[47,48]

There is no rigorous approach to calculate the PCV. Estimated values can be found for known systems in databases. However, for new plane pairs, like in our study, calculations of the *d*-value mismatch are necessary because no data are available for these interface energies.

The calculated *d*-value mismatches between possible matching planes in several systems are reported in Table 1.

Table 1. Calculated *d*-Value Mismatch (%) between Possible Matching Plane Pairs in Several Systems

matching planes	*d*-value mismatch (%)
$\{111\}_{CaB6}/\{1010\}_{NbB2}$	2.9
$\{111\}_{CaB6}/\{1011\}_{NbB2}$	2.8
$\{111\}_{CaB6}/\{1011\}_{TiB2}$	3.15
$\{111\}_{CaB6}/\{1011\}_{VB2}$	1.9
$\{111\}_{CaB6}/\{220\}_{CaF2}$	4.1
$\{111\}_{CaB6}/\{102\}_{CaH2}$	6.2
$\{111\}_{CaB6}/\{200\}_{CaH2}$	6.2
$\{111\}_{CaB6}/\{200\}_{CaO}$	0.14

Determination of the lattice misfit for the $CaF_{2-x}H_x$ phase was not possible due to its unknown stoichiometry. In addition to the transition-metal borides formed by the additives, CaH_2, CaF_2, as well as compounds forming by possible oxygen contamination such as CaO and MgO are evaluated.

Table 1 reports the *d*-value mismatches calculated with respect to the $\{111\}CaB_6$ plane. CaB_6 has a cubic lattice structure (spatial group *Pm*-3*m*) and 4.145 Å as the lattice parameter. The {200}CaO plane provides the lowest *d*-value mismatch (0.14). This value is however misleading because both our experiments[14] and those presented by Kim et al.[10] demonstrate that no reversible formation of $Ca(BH_4)_2$ can be achieved when CaB_6 and CaO (and CaH_2 of course) have to react together to calcium borohydride. Distribution constraints of CaO in the matrix might be at the origin of such an inefficient behavior.

The matching planes were determined with respect to the {1011} plane of the TiB_2 and NbB_2 phase, formed upon desorption of the Nb- and Ti-$Ca(BH_4)_2$ doped system. The {1010} plane of NbB_2 is included as well in Table 1 because it refers to its second most intense XRD reflection (95% of the intensity of the {1011} plane) and therefore the second close-packed plane. TiB_2 (a = 3.032 Å; c = 3.231 Å) and NbB_2 (a = 3.09 Å; c = 3.3 Å) have similar lattice parameters and the same hexagonal lattice structure (space group *P6*/*mmm*). Although the calcium hexaboride structure is different from the one of the transition-metal borides, the $\{111\}CaB_6/\{1011\}NbB_2$, $\{111\}CaB_6/\{1010\}NbB_2$ as well as $\{111\}CaB_6/\{1011\}TiB_2$ plane pairs have the potential to be the matching planes because the *d*-value mismatch is well below the *d*-critical mismatch value (6%). Regarding the results reported in Table 1, a fundamental role of the transition-metal boride nanoparticles as supporters for heterogeneous nucleation is confirmed.

In the case of the $Ca(BH_4)_2$ system milled with TiF_4 and NbF_5, besides TiB_2 and NbB_2 nanoparticles, formation of CaF_2 is observed due to a reaction between the transition-metal fluoride and the borohydride (Supporting Information, Figure 1A and 2A). In the case of the transition-metal fluoride doped MgH_2 system, Jin et al.[49] could not entirely exclude a supportive role of MgF_2 (side product). CaF_2 exhibits a *d*-value mismatch below the critical value, and therefore it should favor the heterogeneous nucleation of CaB_6. The presence of CaB_6 is observed in the XRD pattern in Figure 8 (Des). However, a critical experiment performed adding CaF_2 to $Ca(BH_4)_2$ demonstrated no reversible formation of calcium borohydride after rehydrogenation in the same experimental conditions (350 °C and 145 bar H_2 for 24 h). Further independent experiments with Ti-isopropoxide as additive and no CaF_2 have led to the reversible formation of $Ca(BH_4)_2$ upon rehydrogenation reaction (Figure 5 (Reabs)). This behavior is similar to what was observed for the transition-metal fluoride additives. Hence, we can confirm that CaF_2 does not play any beneficial role in terms of rehydrogenation reaction, but it only exists in the material mixture as a side product. The presence of TiB_2 nanoparticles on the Ti-isopropoxide doped $Ca(BH_4)_2$ material after rehydrogenation reaction is confirmed by SAED (Figure 7). $^{11}B\{^1H\}$ MAS NMR shows CaB_6 after the desorption reaction (Figure 6A). Unfortunately, in our study, there is no analysis confirming the presence of TiB_2 nanoparticles formed upon hydrogen desorption reaction in the case of the Ti-isopropoxide doped sample. However, Deprez et al.[30] reported, for the Ti-isopropoxide doped $2LiBH_4-MgH_2$ composite, that the titanium additive transforms, upon heating, into a mixture of Ti_2O_3 and TiB_2. Simultaneous presence of CaB_6 and TiB_2 nanoparticles in the desorbed material would confirm the same results achieved for the TiF_4 and NbF_5 doped $Ca(BH_4)_2$ system; i.e., transition-metal boride nanoparticles support the heterogeneous nucleation of CaB_6 upon desorption reaction, act as a grain refiner improving the sorption kinetics, and as a consequence, lead to the reversible formation of calcium borohydride. This result is further strengthened observing the $^{11}B\{^1H\}$ MAS NMR spectrum E (Supporting Information, Figure 3) belonging to $Ca(BH_4)_2$ desorbed at 450 °C in vacuum which shows a broad signal at ∼−1 ppm and another less intense one at −33 ppm, corresponding to elemental boron and to residual calcium borohydride, respectively. No significant formation of CaB_6 can be observed. Attempts of rehydrogenation of the desorbed products did not succeed in the reversible formation of $Ca(BH_4)_2$.[14]

Another result that the Ti-isopropoxide doped $Ca(BH_4)_2$ system shares with the TiF_4 and NbF_5 doped materials is a consistent amount of $CaB_{12}H_{12}$ observed after decomposition. In our previous work[14] we observed that the addition of some transition-metal fluorides (TiF_3, VF_3, and VF_4) led to the formation of boron upon desorption besides no visible trace of $CaB_{12}H_{12}$. No reversible formation of $Ca(BH_4)_2$ was observed in that case. The presence of boron would imply that no transition-metal boride nanoparticles are formed, and hence, their absence cannot promote the heterogeneous nucleation of CaB_6. Simultaneous existence of boron and the absence of $CaB_{12}H_{12}$ would suggest that formation of $CaB_{12}H_{12}$ upon desorption is driven by the transition-metal boride nanoparticles. From the results reported in this study, it seems that the almost degenerate decomposition pathways (to CaB_6 and

dx.doi.org/10.1021/jp3116275 | J. Phys. Chem. C 2013, 117, 4394−4403

$CaB_{12}H_{12}$) are followed when transition-metal boride nanoparticles are present.

CONCLUSIONS

A comprehensive investigation of the effect of different selected additives (TiF_4, NbF_5, Ti-isopropoxide, and CaF_2) on the reversible hydrogenation reaction of calcium borohydride was carried out combining different investigation tools.

The formation of TiB_2 and NbB_2 nanoparticles was observed after milling or upon sorption reactions for the Ti- and Nb-based $Ca(BH_4)_2$ doped systems. The formation of nanostructures as well as their good distribution in the material upon cycling was evidenced by TEM measurements.

The positive effect of the Ti-isopropoxide additive on the reversible formation of $Ca(BH_4)_2$ was also highlighted. Instead, the addition of CaF_2 to $Ca(BH_4)_2$ was shown to have no beneficial role in terms of reversible hydrogenation reaction.

CaB_6 is believed to play a key role in promoting the reversible hydrogenation reaction of $Ca(BH_4)_2$. The formation of transition-metal boride nanoparticles during hydrogen desorption is proposed to support the heterogeneous nucleation of CaB_6. The $\{111\}CaB_6/\{1011\}NbB_2$, $\{111\}CaB_6/\{1010\}NbB_2$, as well as $\{111\}CaB_6/\{1011\}TiB_2$ plane pairs have the potential to be the matching planes because the *d*-value mismatch is well below the *d*-critical mismatch value (6%).

Complex hydrides need significant material transport between several solid phases upon rehydrogenation. Therefore, the length scale of the phase separation plays an important role. This aspect becomes even more important when phase segregation occurs. Transition-metal boride nanoparticles act as heterogeneous nucleation sites for CaB_6, refine the microstructure thus improving the sorption kinetics, and, as a consequence, lead to the reversible formation of $Ca(BH_4)_2$.

ASSOCIATED CONTENT

Supporting Information

X-ray diffraction patterns of both $Ca(BH_4)_2$ + 5 mol % NbF_5 and $Ca(BH_4)_2$ + 5 mol % TiF_4 samples collected at different stages of reaction as well as their $^{11}B\{^1H\}$ MAS NMR spectra at room temperature. This material is available free of charge via the Internet at http://pubs.acs.org.

AUTHOR INFORMATION

Corresponding Author

*E-mail: martin.dornheim@hzg.de. Telephone: +49-(0)-4152-87-2604. Fax: +49-(0)-4152-87-2636.

Present Addresses

◊IFW Dresden, Institute for Metallic Materials, Helmholtzstrasse 20, D-01069 Dresden, Germany and Technische Universität Dresden D-01062, Dresden, Germany.

□Dipartimento di Chimica e Farmacia, Universitá di Sassari and INSTM, Via Vienna 2, I-07100 Sassari, Italy.

Notes

The authors declare no competing financial interest.

ACKNOWLEDGMENTS

The authors are grateful to the Marie-Curie European Research Training Network (Contract MRTN- CT-2006-03 5366/COSY) and to the German Bundesministerium für Bildung und Forschung (Förderkennzeichen 03BV108C) for the financial support. E.P., E.R., M.D.B. acknowledge the financial support of 2009-SGR-1292. We thank the Servei de Resonancia Magnetica Nuclear RMN at UAB for their technical assistance. E. Deprez is kindly acknowledged by C.B.M. for useful discussion on XAS data. C.B.M. is grateful to A. Kießling for useful discussions on TEM. M.D.B. thanks partial financial support from an ICREA-Academia award.

REFERENCES

(1) Dornheim, M. Tailoring Reaction Enthalpies of Hydrides. In *Handbook of Hydrogen Storage*; Hirscher, M., Ed.; Wiley-VCH: New York, 2010.

(2) http://www1.eere.energy.gov/hydrogenandfuelcells/stor age/index.html.

(3) Buchter, F.; Łodziana, Z.; Remhof, A.; Friedrichs, O.; Borgschulte, A.; Mauron, Ph.; Züttel, A.; Sheptyakov, D.; Barkhordarian, G.; Bormann, R.; et al. *J. Phys. Chem. B* **2008**, *112*, 8042−8048.

(4) Miwa, K.; Aoki, M.; Noritake, T.; Ohba, N.; Nakamori, Y.; Towata, S.; Zuttel, A.; Orimo, S. *Phys. Rev. B* **2006**, *74*, 155122.

(5) Frankcombe, T. J. *J. Phys. Chem. C* **2010**, *114*, 9503−9509.

(6) Ozolins, V.; Majzoub, E. H.; Wolverton, C. *J. Am. Chem. Soc.* **2009**, *131*, 230−237.

(7) Riktor, M. D.; Sorby, M. H.; Chlopek, K.; Fichtner, M.; Buchter, F.; Züttel, A.; Hauback, B. C. *J. Mater. Chem.* **2007**, *17*, 4939−4942.

(8) Wang, L. L.; Graham, D. D.; Robertson, I. M.; Johnson, D. D. *J. Phys. Chem. C* **2009**, *113*, 20088−20096.

(9) Zhang, Y. S.; Majzoub, E.; Ozolins, V.; Wolverton, C. *Phys. Rev. B* **2010**, *82*, 174107.

(10) Kim, Y.; Reed, D.; Lee, Y. S.; Lee, J. Y.; Shim, J. H.; Book, D.; Cho, Y. W. *J. Phys. Chem. C* **2009**, *113*, 5865−5871.

(11) Sivaev, I. B.; Sjoberg, S.; Bregadze, V. I.; Gabel, D. *Tetrahedron Lett.* **1999**, *40*, 3451−3454.

(12) Riktor, M. D.; Sorby, M. H.; Chlopek, K.; Fichtner, M.; Hauback, B. C. *J. Mater. Chem.* **2009**, *19*, 2754−2759.

(13) Lee, J. Y.; Ravnsbaek, D.; Lee, Y. S.; Kim, Y.; Cerenius, Y.; Shim, J. H.; Jensen, T. R.; Hur, N. H.; Cho, Y. W. *J. Phys. Chem. C* **2009**, *113*, 15080−15086.

(14) Bonatto Minella, C.; Garroni, S.; Pistidda, C.; Gosalawit-Utke, R.; Barkhordarian, G.; Rongeat, C.; Lindemann, I.; Gutfleisch, O.; Jensen, T. R.; Cerenius, Y.; et al. *J. Phys. Chem. C* **2011**, *115*, 2497−2504.

(15) Kim, Y.; Reed, D.; Lee, Y. S.; Lee, J. Y.; Shim, J. H.; Book, D.; Cho, Y. W. *J. Phys. Chem. C* **2009**, *113*, 5865−5871.

(16) Bonatto Minella, C.; Garroni, S.; Olid, D.; Teixidor, F.; Pistidda, C.; Lindemann, I.; Gutfleisch, O.; Baró, M. D.; Bormann, R.; Klassen, T.; et al. *J. Phys. Chem. C* **2011**, *115*, 18010−18014.

(17) Barkhordarian, G.; Klassen, T.; Bormann, R. *Scr. Mater.* **2003**, *49*, 213−217.

(18) Bogdanovic, B.; Schwickardi, M. *J. Alloys Compd.* **1997**, *253*, 1−9.

(19) Fang, Z. Z.; Ma, L. P.; Kang, X. D.; Wang, P. J.; Wang, P.; Cheng, H. M. *Appl. Phys. Lett.* **2009**, *94*, 044104.

(20) Ronnebro, E.; Majzoub, E. H. *J. Phys. Chem. B* **2007**, *111*, 12045−12047.

(21) Rongeat, C.; D'Anna, V.; Hagemann, H.; Borgschulte, A.; Züttel, A.; Schultz, L.; Gutfleisch, O. *J. Alloys Compd.* **2010**, *493*, 281−287.

(22) Kim, J. H.; Jin, S. A.; Shim, J. H.; Cho, Y. W. *Scr. Mater.* **2008**, *58*, 481−483.

(23) Kim, J. H.; Shim, J. H.; Cho, Y. W. *J. Power Sources* **2008**, *181*, 140−143.

(24) Jin, S. A.; Shim, J. H.; Ahn, J. P.; Cho, Y. W.; Yi, K. W. *Acta Mater.* **2007**, *55*, 5073−5079.

(25) Wang, X. L.; Suda, S. *J. Alloys Compd.* **1995**, *231*, 380−386.

(26) Ivanov, E.; Konstanchuk, I.; Bokhonov, B.; Boldyrev, V. *J. Alloys Compd.* **2003**, *359*, 320−325.

(27) Friedrichs, O.; Aguey-Zinsou, F.; Fernández, J. R. A.; Sánchez-López, J. C.; Justo, A.; Klassen, T.; Bormann, R.; Fernández, A. *Acta Mater.* **2006**, *54*, 105−110.

(28) Friedrichs, O.; Martínez-Martínez, D.; Guilera, G.; Sánchez López, J. C.; Fernández, A. *J. Phys. Chem. C* **2007**, *111*, 10700−10706.
(29) Friedrichs, O.; Sánchez-López, J. C.; López-Cartes, C.; Klassen, T.; Bormann, R.; Fernández, A. *J. Phys. Chem. B* **2006**, *110*, 7845−7850.
(30) Deprez, E.; Munoz-Marquez, M. A.; Roldan, M. A.; Prestipino, C.; Palomares, F. J.; Bonatto Minella, C.; Bosenberg, U.; Dornheim, M.; Bormann, R.; Fernandez, A. *J. Phys. Chem. C* **2010**, *114*, 3309−3317.
(31) Deprez, E.; Munoz-Marquez, M. A.; de Haro, M. C. J.; Palomares, F. J.; Soria, F.; Dornheim, M.; Bormann, R.; Fernandez, A. *J. Appl. Phys.* **2011**, *109*, 014913.
(32) Bösenberg, U.; Vainio, U.; Pranzas, P. K.; Bellosta von Colbe, J. M.; Goerigk, G.; Welter, E.; Dornheim, M.; Schreyer, A.; Bormann, R. *Nanotechnology* **2009**, *20*, 204003.
(33) Bösenberg, U.; Kim, J. W.; Gosslar, D.; Eigen, N.; Jensen, T. R.; von Colbe, J. M. B.; Zhou, Y.; Dahms, M.; Kim, D. H.; Gunther, R.; et al. *Acta Mater.* **2010**, *58*, 3381−3389.
(34) Ravel, B.; Newville, M. *J. Synchrotron Radiat.* **2005**, *12*, 537−541.
(35) Newville, M. *J. Synchrotron Radiat.* **2001**, *8*, 322−324.
(36) Cerenius, Y.; Stahl, K.; Svensson, L. A.; Ursby, T.; Oskarsson, A.; Albertsson, J.; Liljas, A. *J. Synchrotron Radiat.* **2000**, *7*, 203−208.
(37) Lutterotti, L.; Matthies, S.; Wenk, H. R.; Schultz, A. S.; Richardson, J. W. *J. Appl. Phys.* **1997**, *81*, 594−600.
(38) Takacs, L.; McHenry, J. S. *J. Mater. Sci.* **2006**, *41*, 5246−5249.
(39) Konings, R. *Struct. Chem.* **1994**, *5*, 9−13.
(40) Züttel, A.; Borgschulte, A.; Orimo, S. I. *Scr. Mater.* **2007**, *56*, 823−828.
(41) Riktor, M. D.; Filinchuk, Y.; Vajeeston, P.; Bardaji, E. G.; Fichtner, M.; Fjellvag, H.; Sorby, M. H.; Hauback, B. C. *J. Mater. Chem.* **2011**, *21*, 7188−7193.
(42) Buslaev, Y. A.; Dyer, D. S.; Ragsdale, R. O. *Inorg. Chem.* **1967**, *6*, 2208−2212.
(43) Ngene, P.; Verkuijlen, M. H. W.; Zheng, Q.; Kragten, J.; van Bentum, P. J. M.; Bitter, J. H.; de Jongh, P. E. *Faraday Discuss.* **2011**, *151*, 47−58.
(44) Hwang, S. J.; Bowman, R. C.; Reiter, J. W.; Rijssenbeek, J.; Soloveichik, G. L.; Zhao, J. C.; Kabbour, H.; Ahn, C. C. *J. Phys. Chem. C* **2008**, *112*, 3164−3169.
(45) Pistidda, C.; Garroni, S.; Bonatto Minella, C.; Dolci, F.; Jensen, T. R.; Nolis, P.; Bösenberg, U.; Cerenius, Y.; Lohstroh, W.; Fichtner, M.; et al. *J. Phys. Chem. C* **2010**, *114*, 21816−21823.
(46) Bösenberg, U. $LiBH_4$-MgH_2 Composites for Hydrogen Storage. *Ph.D. Dissertation*, Technische Universität Hamburg-Harburg, Hamburg, 2009.
(47) Zhang, M. X.; Kelly, P. M. *Scr. Mater.* **2005**, *52*, 963−968.
(48) Kelly, P. M.; Zhang, M. X. *Metall. Mater. Trans. A* **2006**, *37*, 833−839.
(49) Jin, S. A.; Shim, J. H.; Ahn, J. P.; Cho, Y. W.; Yi, K. W. *Acta Mater.* **2007**, *55*, 5073−5079.